Hindawi Publishing Corporation
Mathematical Problems in Engineering
Volume 2014, Article ID 821689, 10 pages
http://dx.doi.org/10.1155/2014/821689

Research Article

Numerical Investigation of Wave Slamming of Flat Bottom Body during Water Entry Process

Xiaozhou Hu and Shaojun Liu

School of Mechanical and Electrical Engineering, Central South University, Changsha 410083, China

Correspondence should be addressed to Xiaozhou Hu; smallboathu@163.com

Received 23 December 2013; Revised 4 April 2014; Accepted 8 April 2014; Published 29 April 2014

Academic Editor: Benchawan Wiwatanapataphee

A numerical wave load model based on two-phase (water-air) Reynolds-averaged Navier-Stokes (RANS) type equations is used to evaluate hydrodynamic forces exerted on flat bottom body while entering ocean waves of deploying process. The discretization of the RANS equations is achieved by a finite volume (FV) approach. The volume of fluid (VOF) method is employed to track the complicated free surface. A numerical wave tank is built to generate the ocean waves which are suitable for deploying offshore structures. A typical deploying condition is employed to reflect the process of flat bottom body impacting waves, and the pressure distribution of bottom is also presented. Four different lowering velocities are applied to obtain the relationship between slamming force and wave parameters. The numerical results clearly demonstrated the characteristics of flat bottom body impacting ocean waves.

1. Introduction

At the beginning of deployment of offshore structures, the wave impact load due to slamming between the deployed bodies and free surface of ocean wave is a dangerous phenomenon, which attracts more and more attention from ocean engineering field. Firstly, wave impact is a strong nonlinear phenomenon and a random process which is very sensitive to relative motion between body and free surface, and the deployed bodies undergo hydrodynamic loads that may induce localized plastic deformation even catastrophic damage in hostile sea conditions. Secondly, during the process of water entering ocean waves, the nonlinear interaction between deployed bodies and waves may result in dynamic tension of deploying cable which connects the deployed bodies and crane equipment, even leading to fracture of cable and missing of deployed bodies. Therefore, it is significant to predict the whole water entry process of flat bottom body, as well as the pressure distribution and maximum impact pressure on the body, which is the practical motivation for the theoretical and numerical studies in this paper.

Slamming phenomena have been studied over several decades especially in naval hydrodynamics. Pioneering research had been carried out by Von Karman [1], Wanger [2], Chuang [3], and Zhao and Faltinsen [4]. These studies mainly focused on the calculation of slamming force without considering the effect of ocean waves.

Concerning the wave impact of flat bottom body in deploying process, the present solution is empirical equations [5]. Although available empirical equations from laboratory prototype experiments can be used to get approximate estimations of wave impact forces on deployed flat bottom body, the nonlinear influence of ocean waves on body is difficult to evaluate. Also, most empirical equations provide only maximum values of wave forces rather than the force time history.

In this regard, numerical modeling of wave loads on deployed flat bottom body is a very useful supplementary approach for estimating wave loads. With the development of computer hardware and computational fluid dynamics, numerical methods have been extensively used to solve the water entry of rigid body under fully nonlinear free surface conditions.

Recently, there are many significant studies concerning related problems, which are introduced as follows.

Baarholm and Faltinsen [6] used a boundary element model to study water impacts on a fixed horizontal platform deck from regular incident waves. They simplified this problem to a two-dimensional potential flow problem and solved the resulting boundary value problem by three different numerical methods: simplified Wagner-based method and two boundary element methods solving the perturbation velocity potential due to the impact and the total velocity potential, respectively. Chen and Xiao [7] used commercial software MSC Dytran to study the water entry of flat-bottom structure with constant velocity, and air cushion and splash were observed. Bunnik and Buchner [8, 9] applied the improved volume of fluid (iVOF) method for better numerical prediction of the behavior of a subsea structure in the splash zone; dedicated model tests verified simulations. Ding et al. [10] presented the experimental investigation of unidirectional random wave slamming on the three-dimensional structure in the splash zone. Sarkar and Gudmestad [11] discussed the hydrodynamic coefficients (drag coefficients and added mass coefficients) and analysis methodology for the splash zone deploying analysis. Zhang et al. [12] built a model of fluid with CFD software to analyze the dynamic character of the deployment and retrieval system, when it was deployed into water and retrieved out of water without considering the effect of ocean waves. Chen and Yu [13] implemented CFD simulation of wet deck slamming with interface-preserving level-set method. W.-H. Wang and Y.-Y. Wang [14, 15] used a CFD method to numerically simulate the physical process of cylinder vertically entering water in regular waves, and the effect of wave parameters on the hydrodynamic force was analyzed.

Accordingly, in this work, regular waves of ocean conditions (4–6 degrees) which are for the deployment of offshore structures are generated in a numerical wave tank, and their properties and sensitivity to governing parameters are investigated.

This paper is motivated by developing a practical method in simulating the wave slamming of flat bottom body based on the CFD solver Fluent. It is organized as follows: the wave model equations and numerical methods implemented in the simulation are described in Section 2, including governing equations, boundary conditions, generation of waves, and numerical wave-absorbing beach, as well as parameters and mesh of numerical wave tank; numerical experiments and results, together with their physical interpretation, are presented in Section 3.

2. The Numerical Method

2.1. Governing Equations. For simulations of water surface waves, the Navier-Stokes equation-based model is known as one of the numerical models capable of overcoming the limitations of nonlinearity, dispersion, and wave breaking, which most of the conventional wave models cannot do. Therefore, the CFD calculations of this paper are based on the RANS equations. The flow of a homogeneous, incompressible, viscous fluid is described by the Navier-Stokes equations, respectively; they are given by

$$\frac{\partial \rho}{\partial t} + \frac{\partial (\rho u_i)}{\partial x_i} = 0, \quad (i = 1, 2),$$
$$\frac{\partial (\rho u_i)}{\partial t} + u_j \frac{\partial (\rho u_i)}{\partial x_i} = \frac{\partial}{\partial x_j}\left[\mu\left(\frac{\partial u_i}{\partial x_j} + \frac{\partial u_j}{\partial x_i}\right)\right] - \frac{\partial p}{\partial x_i} + \rho f_i, \tag{1}$$

where $i, j = 1, 2$ for two-dimensional flows, $u_i = i$th component of the velocity vector, ρ is the density of fluid, p is the pressure, μ is the dynamic viscous coefficient, and f_i is the body force.

By implementing the Reynolds decomposition in the N-S equations and averaging, the Reynolds-averaged Navier-Stokes (RANS) equations governing the average flow field are derived:

$$\frac{\partial (\rho \overline{u}_i)}{\partial t} + \frac{\partial \left(\rho \overline{u}_i \overline{u}_j\right)}{\partial x_i} = -\frac{\partial \overline{p}}{\partial x_i} + \frac{\partial}{\partial x_j}\left[\mu\left(\frac{\partial \overline{u}_i}{\partial x_j} + \frac{\partial \overline{u}_j}{\partial x_i}\right)\right] + \frac{\partial}{\partial x_j}\left(-\rho \overline{u_i'}\, \overline{u_j'}\right) + \rho \overline{f}_i, \tag{2}$$

where the superscripts "—" denote ensemble average of the physical variables and $-\rho \overline{u_i'} \overline{u_i'}$ is the Reynolds stress.

In this paper, the standard k–ε model, where the Reynolds stress is approximated by a nonlinear algebraic stress model, is employed for turbulence closure. The governing equations for k and ε model are given by

$$\frac{\partial (\rho k)}{\partial t} + \frac{\partial \left(\rho k \overline{u}_j\right)}{\partial x_i} = \frac{\partial}{\partial x_j}\left[\left(\mu + \frac{\mu_t}{\sigma_k}\right)\frac{\partial k}{\partial x_j}\right] + \rho G_k - \rho \varepsilon, \tag{3}$$

$$\frac{\partial (\rho \varepsilon)}{\partial t} + \frac{\partial \left(\rho \varepsilon \overline{u}_j\right)}{\partial x_i} = \frac{\partial}{\partial x_j}\left[\left(\mu + \frac{\mu_t}{\sigma_\varepsilon}\right)\frac{\partial k}{\partial x_j}\right] + \frac{\varepsilon}{k}\left(C_{\varepsilon 1}\rho G_k - C_{\varepsilon 2}\rho \varepsilon\right), \tag{4}$$

$$\mu_t = \frac{C_\mu \rho k^2}{\varepsilon}, \tag{5}$$

$$G_k = \frac{\mu_t}{\rho}\left(\frac{\partial \overline{u}_i}{\partial x_j} + \frac{\partial \overline{u}_j}{\partial x_i}\right)\frac{\partial \overline{u}_i}{\partial x_j}, \tag{6}$$

where k is the turbulence kinetic energy, ε is the dissipation rate of turbulence kinetic energy, μ_t is the eddy viscosity, and G_k is the turbulent energy production.

The empirical coefficients in (3)–(5) have been determined by performing many simple experiments and enforcing the physical realizability condition; the values are given as follows:

$$C_\mu = 0.09, \quad C_{\varepsilon 1} = 1.44, \quad C_{\varepsilon 2} = 1.92, \quad \sigma_k = 1.0, \quad \sigma_\varepsilon = 1.3. \tag{7}$$

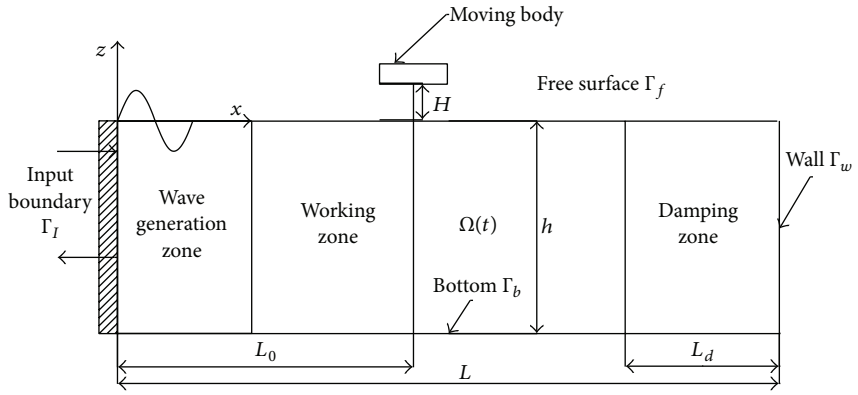

Figure 1: Numerical wave tank and moving body.

The VOF method is employed to track the complicated free surface, with a volume of fluid function F to define the water region. The physical meaning of the F function is the fractional volume of a cell occupied by water, with unity to represent a cell full of water and zero for a cell with no water. Cells with F values between zero and unity must then contain the free surface.

If the volume fraction of water and air in each cell is denoted as a_w and a_a, respectively, the tracking of the interface between the phases is accomplished by the solution of a continuity equation for the volume fraction of water.

This equation of a_w has the following form:

$$\frac{\partial a_w}{\partial t} + u_i \frac{\partial (a_w)}{\partial x_i} = 0. \tag{8}$$

The volume fraction equation will not be solved for air; the volume fraction of air will be computed based on the following constraint:

$$a_w + a_a = 1. \tag{9}$$

For (9), $a_w = 0$ means air phase and $a_a = 0$ means water phase, while $a_a = 0$~1 means the mixture phase.

2.2. Boundary Conditions

2.2.1. Free Surface Boundary Conditions. Dynamic free surface condition can be written as

$$\frac{\partial \phi}{\partial t} = -g\eta - \frac{1}{2}\left|\nabla\phi\right|^2 - \frac{P_a}{\rho}, \tag{10}$$

where P_a is the pressure on the free surface and is assumed to be zero from now on.

And kinematic free surface condition can be written as

$$\frac{\partial \eta}{\partial t} = -\nabla\phi \cdot \nabla\eta + \frac{\partial \phi}{\partial z}. \tag{11}$$

Both the dynamic and kinematic free surface boundary conditions are satisfied on the exact free surface.

2.2.2. Bottom Boundary Condition. No normal-flux condition is applied on the bottom of numerical wave tank. Consider

$$\frac{\partial \phi}{\partial n} = 0. \tag{12}$$

2.2.3. Body Boundary Condition. The body boundary condition is written as

$$\frac{\partial \phi}{\partial n} = V \cdot n, \tag{13}$$

where V and n are body velocity with respect to gravity center and surface normal vector of body, respectively.

2.2.4. Wall Boundary Condition. The solution domain is bounded by a wave-maker on the left wall boundary. At the wave-maker boundary, the horizontal velocity of motion of the boundary is imposed on the water particle velocities at the boundary, as shown in Figure 1.

No-slip condition is applied on the right vertical wall of numerical wave tank. Consider

$$\frac{\partial \phi}{\partial n} = 0. \tag{14}$$

The no-slip condition ensures that the fluid moving over a solid surface does not have velocity relative to the surface at the point of contact.

2.3. Generation of Waves and Numerical Wave-Absorbing Beach. The piston wave-maker is employed to generate waves in this paper. A schematic diagram of a numerical wave tank with piston wave-maker is shown in Figure 1.

The waves are generated by a piston type wave-maker located at the left boundary of the solution domain. If the plunger moves sinusoidally with the function

$$X(t) = \frac{X_0}{2} \sin \omega t, \tag{15}$$

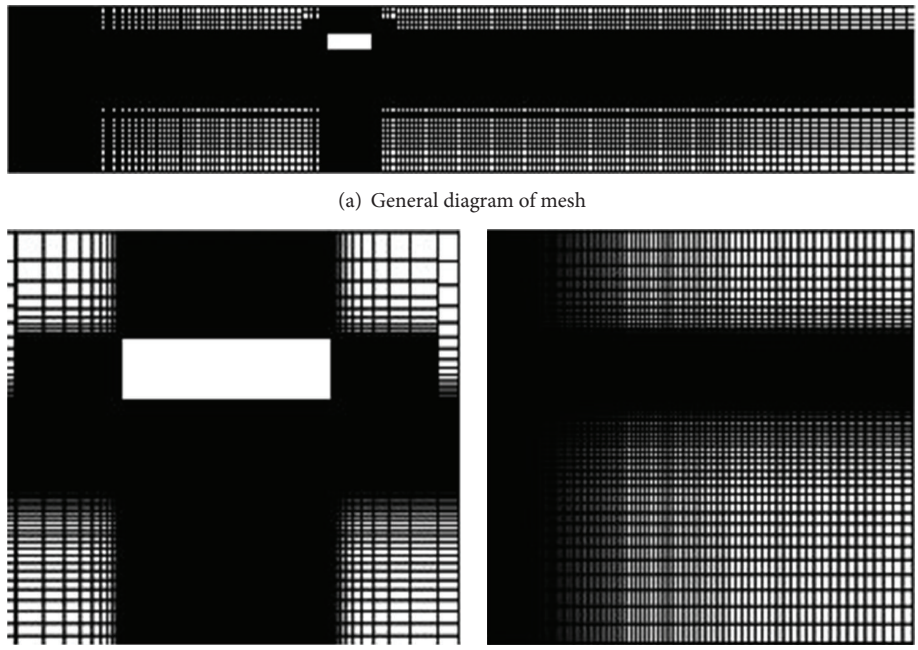

(a) General diagram of mesh

(b) Mesh surrounding moving body

(c) Mesh near wave-maker

Figure 2: Schematic diagrams of mesh.

where X_0 is the maximum horizontal displacement of plunger and ω is the angular frequency of motion, then the wave free surface equation is as follows:

$$\eta(x,t) = \frac{X_0}{2}\left(\frac{4\sinh^2 kd}{2kd+\sinh 2kd}\cos(kx-\omega t) + \sum_{n=1}^{\infty}\frac{4\sin^2(k_n d)}{2k_n d+\sin(2k_n d)}e^{-k_n x}\sin\omega t\right), \tag{16}$$

where d is the water depth and k is the wave number.

The first part of (16) is the incoming wave with wave number k and the angular frequency is ω, and the second part is attenuating standing wave induced by the piston. If the second part of (16) can be eliminated, the surface elevation equation can be given:

$$\eta(x,t) = \frac{X_0}{2}\frac{4\sinh^2 kd}{2kd+\sinh 2kd}\cos(kx-\omega t) = \frac{H}{2}\cos(kx-\omega t), \tag{17}$$

where Hcan be obtained:

$$H = \frac{4\sinh^2(kd)}{2kd+\sinh(2kd)}X_0. \tag{18}$$

Nonreflecting boundaries have to be used or a damping/dissipation zone is added to the solution domain for damping the waves. In this work, towards the end of the computational domain, the porous media technology is applied to form an artificial damping zone so that the wave energy is gradually dissipated in the direction of wave propagation.

The porous media are modeled by the addition of a momentum source term to the standard fluid flow equations; the momentum source term of simple homogeneous porous media can be written as follows:

$$S_i = -\left(\frac{\mu}{\alpha}v_i + C_2\frac{1}{2}\rho|v_i|v_i\right), \tag{19}$$

where S_i is the source term for the ith (x, y, or z) momentum equation, $|v_i|$ is the magnitude of the velocity, μ is the viscosity of the fluid, C_2 is the inertial resistance factor, and α is the permeability which is a measure of the ability of porous material to transmit fluids. The determination methods of permeability for different waves can refer to Hu et al.'s work [16]. Besides, the length of the damping zone is determined to be at least 2 wavelengths.

2.4. Parameters and Mesh of Numerical Wave Tank. The 2D numerical tank is set as a rectangle with 300 m length and 30 m height, and the width (B) and height of deployed body are 10 m and 3 m. The still water depth (d) is set as 20 m. The numerical grid exported by Gambit is shown in Figure 2; the grid sizes are nonuniform and change case by case according to the wavelength and the water depth. The general rule for constructing grids is to make them denser for the shoaling and wave breaking region near the water surface.

3. Numerical Experiments

3.1. Verification of Numerical Wave Tank. A regular wave with wave height 2.5 m and period 6 s which is suitable for deployment of offshore structures is used to verify the effectiveness and correctness of numerical wave tank introduced

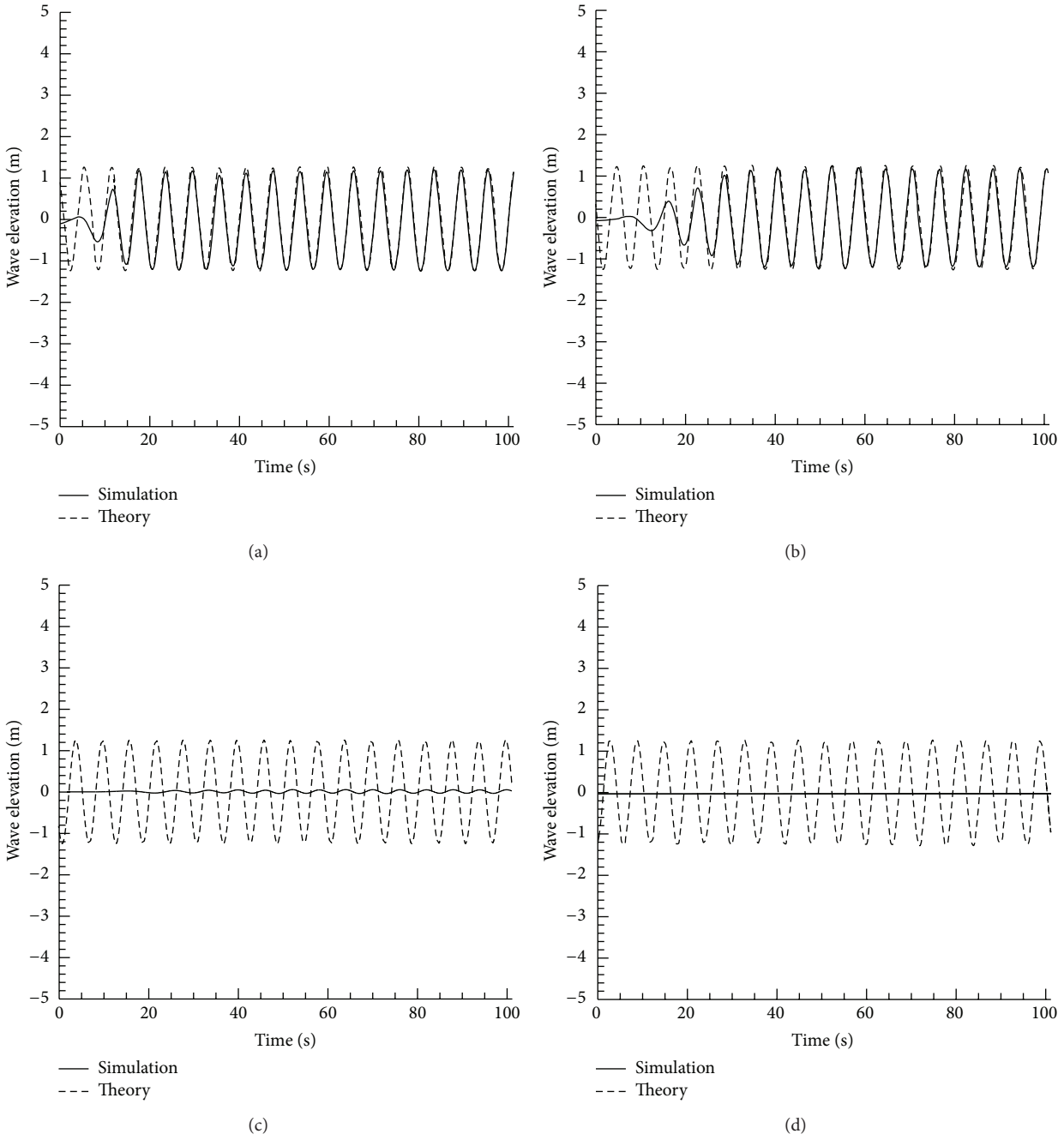

Figure 3: Wave elevation at four different locations: (a) $x = 50$ m; (b) $x = 100$ m; (c) $x = 200$ m; (d) $x = 300$ m.

in Section 2. A user defined function (UDF) implements the numerical wave generation and absorbing approach. The simulation parameters are as follows: permeability of porous zone $\alpha = 1 \times 10^{-6}$; the length of porous zone is determined as 150 m. Wave elevations of locations of $x = 50$ m, 100 m, 200 m, and 300 m are determined as wave elevation probes; wave elevations of each ocean condition are compared with the corresponding analytical solutions.

The simulated waves are shown in Figure 3. From Figure 3, it can be seen that wave elevations of working zone of wave tank ($x = 50$ m, 100 m) are almost identical with the analytical solutions, which means that the error between simulation results and analytical solutions is very small and that the reflected waves are eliminated. Besides, Figure 3 also reflects that the wave energy in damping zone of wave tank ($x = 200$ m and 300 m) has been absorbed; that is to say, the amplitude attenuation rate is 100%. Therefore, it can be concluded that the performance of numerical wave tank is perfect and can satisfy the demand of studying water-entry of flat bottom body in ocean waves numerically.

3.2. Numerical Example of Flat Bottom Body Impacting Waves. A numerical example is performed to show the whole water entry process of flat bottom body in wave. The main information of numerical example is as follows: the wave height and period of aimed wave are 2.5 m and 8 s, respectively; the constant vertical velocity of body is $v_d = 2$ m/s; the initial time of simulation is $t_0 = 0$ s, and the motion of wave-maker will make aimed waves from the initial time; the initial moving time of flat bottom body is $T_0 = 19.31$ s.

The phase diagrams and pressure distribution diagrams of bottom of $T = 20.412$ s, 20.462 s, 20.612 s, and 20.658 s are shown in Figure 4. These figures can clearly reflect the whole water entry process of flat bottom body in wave. At $T = 20.412$ s, the left part of flat bottom body impacts the wave surface, and, with wave continuing to propagate to the right, the contact length between wave and body is increasing. According to Hu and Liu [17], when flat bottom body enters calm water, some phenomena can be observed: firstly, the air cushioning effect exists when the air is trapped between the falling flat bottom body and the fluid, which is also mentioned by Faltinsen [18]; secondly, the impact pressure distribution of bottom is axis-symmetric, and the maximum pressure appears at the center of bottom. Compared with the clam water entry case, the case of entering water in wave is totally different: as shown in Figure 4, impact pressure distribution of bottom is nonsymmetric, and the maximum pressure appears at the interface between rigid body (the flatted bottom body) and two-phase fluid (water and air); besides, the pressure of bottom getting in contact with water is much bigger than that getting in contact with air, and the trapped air between body bottom and fluid is relatively limited (it is determined by the length of bottom), which will be discussed in Section 3.3.

3.3. Slamming Force Analysis. During the transit of the structure through the wave surface, high slamming force may occur; thus, it is important to evaluate impact load. The slamming coefficient of flat bottom body can be defined, which is nondimensional impact force, similar to that of circular cylinder.

The slamming coefficient C_s is defined as

$$C_s = \frac{F_s}{\rho_w v_d^2 B}, \tag{20}$$

where F_s is the maximum slamming force during water entry process, ρ_w is the density of ocean water, v_d is the deploying velocity, and B is the width of flat bottom body.

In the numerical experiments, four different velocities of body are 1, 2, 3, and 4 m/s. To investigate the influence that wave height and period exert on slamming force, the coefficient H/d which is the ratio between wave height (H) and water depth (d) is employed, as well as B/L which is the ratio between length (B) of deployed body and wave length (L). Waves with different heights (H) and wave lengths (L) are selected so as to study the relationship between slamming coefficient and coefficients B/L and H/d, which are shown in Table 1.

Table 1: Parameters of numerical experiments.

Parameters	Values					
H (m)	1	2	3	4	5	6
H/d	0.05	0.1	0.15	0.2	0.25	0.3
T (s)	3	4	6	8	10	12
L (m)	14	25	55	88.7	121.2	153.2
B/L	0.714	0.4	0.182	0.113	0.083	0.065

Related researches reflect that the wave height plays an important role in affecting wave impact force [10]. Figure 5 shows the relationship between H/d and slamming coefficients with different deploying velocities and B/L.

As shown in Figure 5, when the body impacts ocean waves, the slamming coefficient increases with H/d increasing, while it decreases rapidly with deploying velocity increasing, which is similar to the case in which the body impacts calm water; however, the slamming coefficient of the latter case is explicitly smaller than the former one.

Most pioneer experimental and numerical researches favor the suppose that the maximum impact pressure is approximately proportional to the square of the relative impact velocity V_0 [3, 7]; thus, (20) can be rewritten as

$$C_s = \frac{F_s}{\rho_w v_d^2 B} = \frac{F_s\left(V_0^2\right)}{\rho_w v_d^2 B}, \qquad V_0 = v_d + v_w, \tag{21}$$

where v_w is instantaneous velocity of water particles in vertical direction. For regular, waves, v_w is determined by H and T, and it is clear that slamming coefficient C_s increases with the ratio v_w/v_d increasing.

B/L is also an important factor which determines the slamming force. As shown in Figure 4, when the bottom of the deployed body impacts wave, the length of the bottom is the displacement that the wave travels and it also affects the compression level of trapped air between body bottom and fluid. Figure 6 shows the relationship between B/L and slamming coefficients with different deploying velocities and H/d.

As can be seen in Figure 6, slamming coefficient increases with B/L increasing, which is due to air cushioning effect which is also mentioned by Chuang [3] and Chen et al. [19]. For different deploying velocities, the same law can be seen: when B/L is small, C_s increases slowly; comparatively, when B/L is bigger than 0.2, C_s changes rapidly.

4. Conclusion

The numerical wave-load model based on Navier-Stokes type equations and the VOF method has been applied to investigate the dynamic impact of wave forces on flat bottom body during its deploying process. Based on the statistical analysis of the simulation results, the following conclusions can be listed.

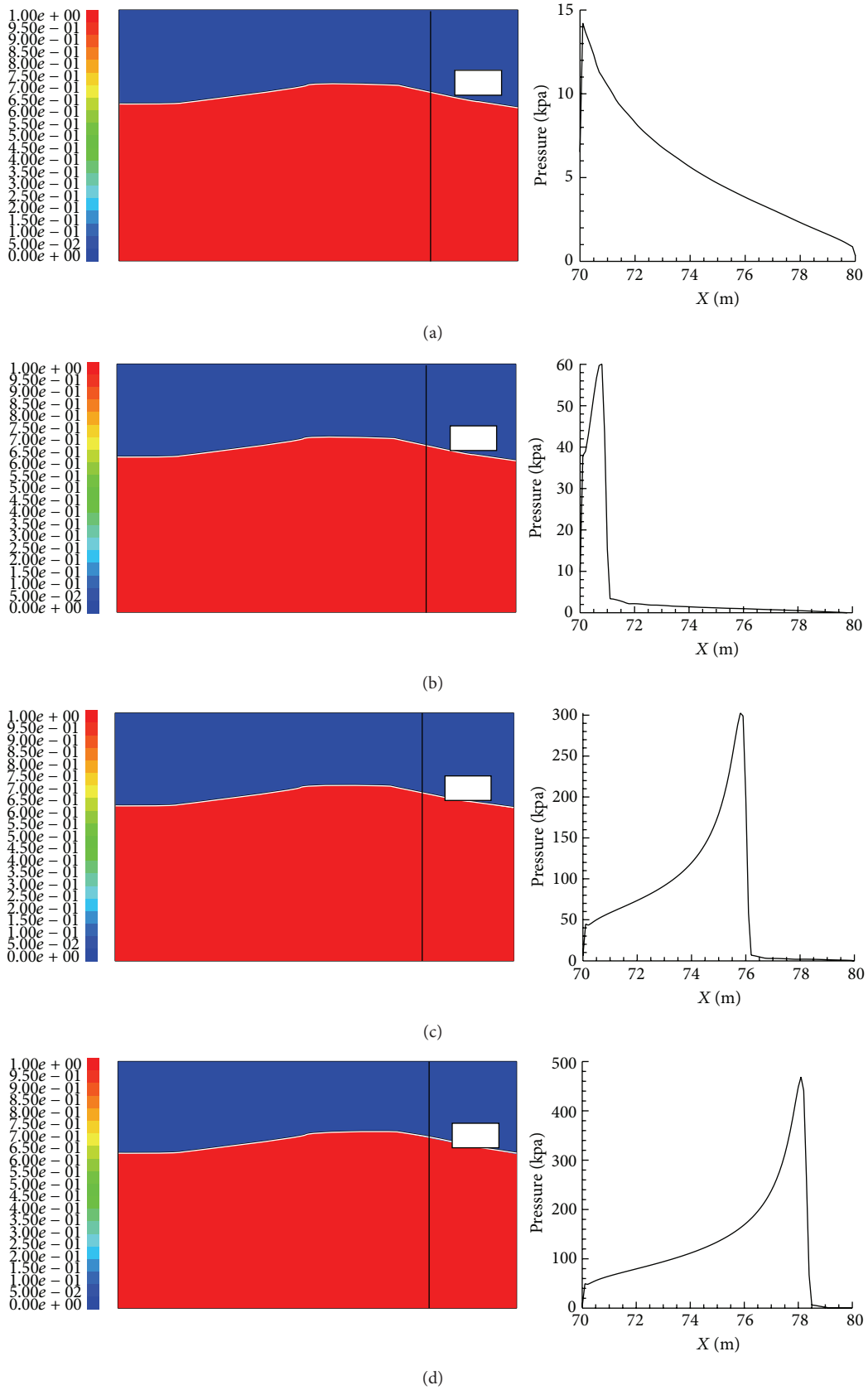

Figure 4: Phase diagram of the flow field and pressure profile at the body bottom at four different times: (a) $T = 20.412$ s; (b) $T = 20.462$ s; (c) $T = 20.612$ s; (d) $T = 20.658$ s.

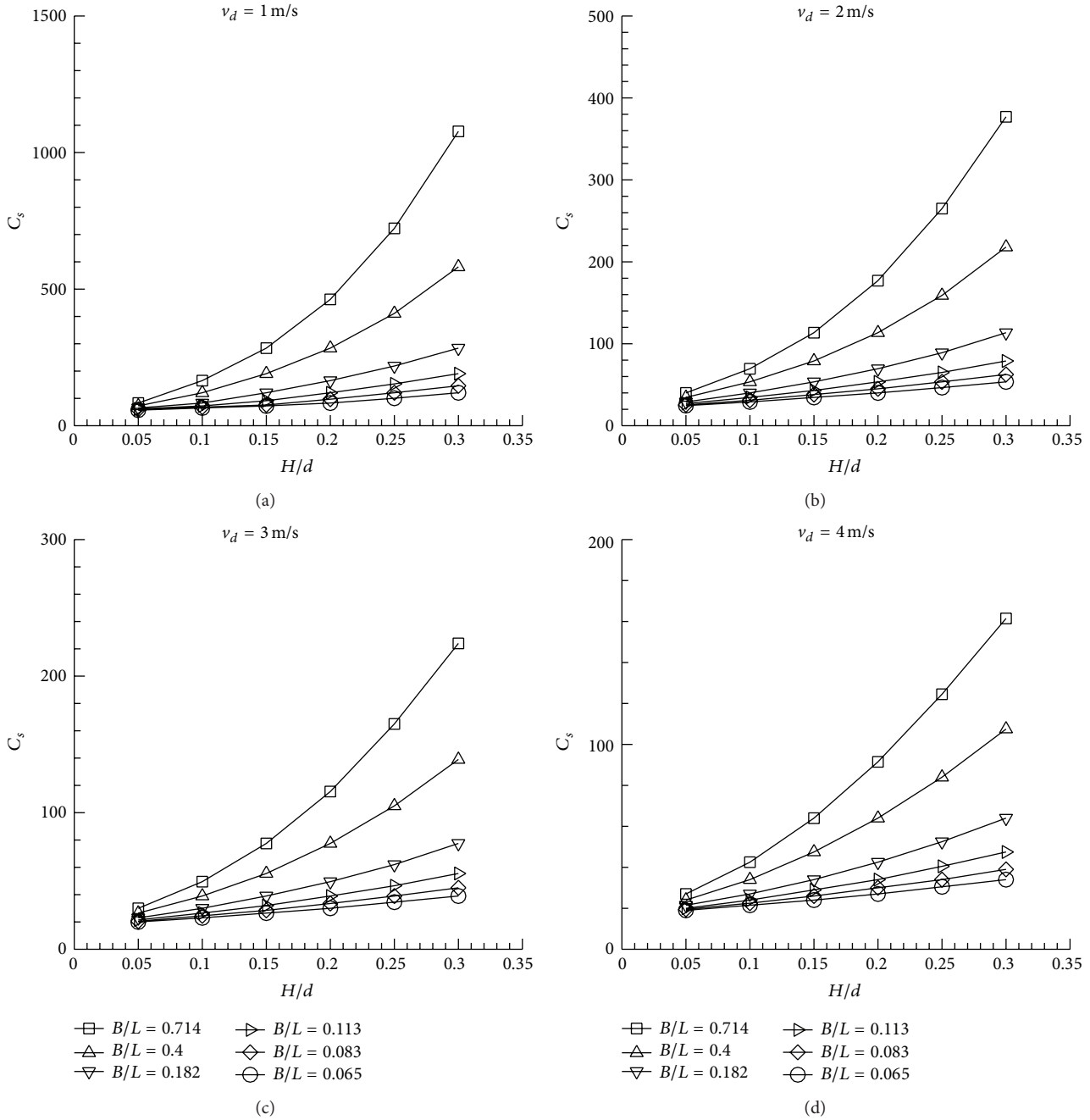

Figure 5: Relationship between slamming coefficient and H/d.

(1) Waves which are generated based on piston type wave-maker method and porous media wave absorption method clearly demonstrate the flexibility and accuracy of this type of numerical wave tank for simulating kinds of waves of different ocean conditions; thus, it can be used for studying the impact load between flat bottom body and ocean waves in its deployment.

(2) The impact pressure distribution of bottom is nonsymmetric, and the maximum pressure appears at the interface between rigid body and two-phase fluid; the pressure of bottom getting in contact with water is much bigger than that getting in contact with air.

(3) The slamming coefficient increases with H/d or B/L increasing, while it decreases with deploying velocity increasing, which means that H/d, B/L, and the deploying velocity can exert great influence on the wave impact force.

(4) This study can be a reference for studying the interaction between flat bottom body and ocean waves

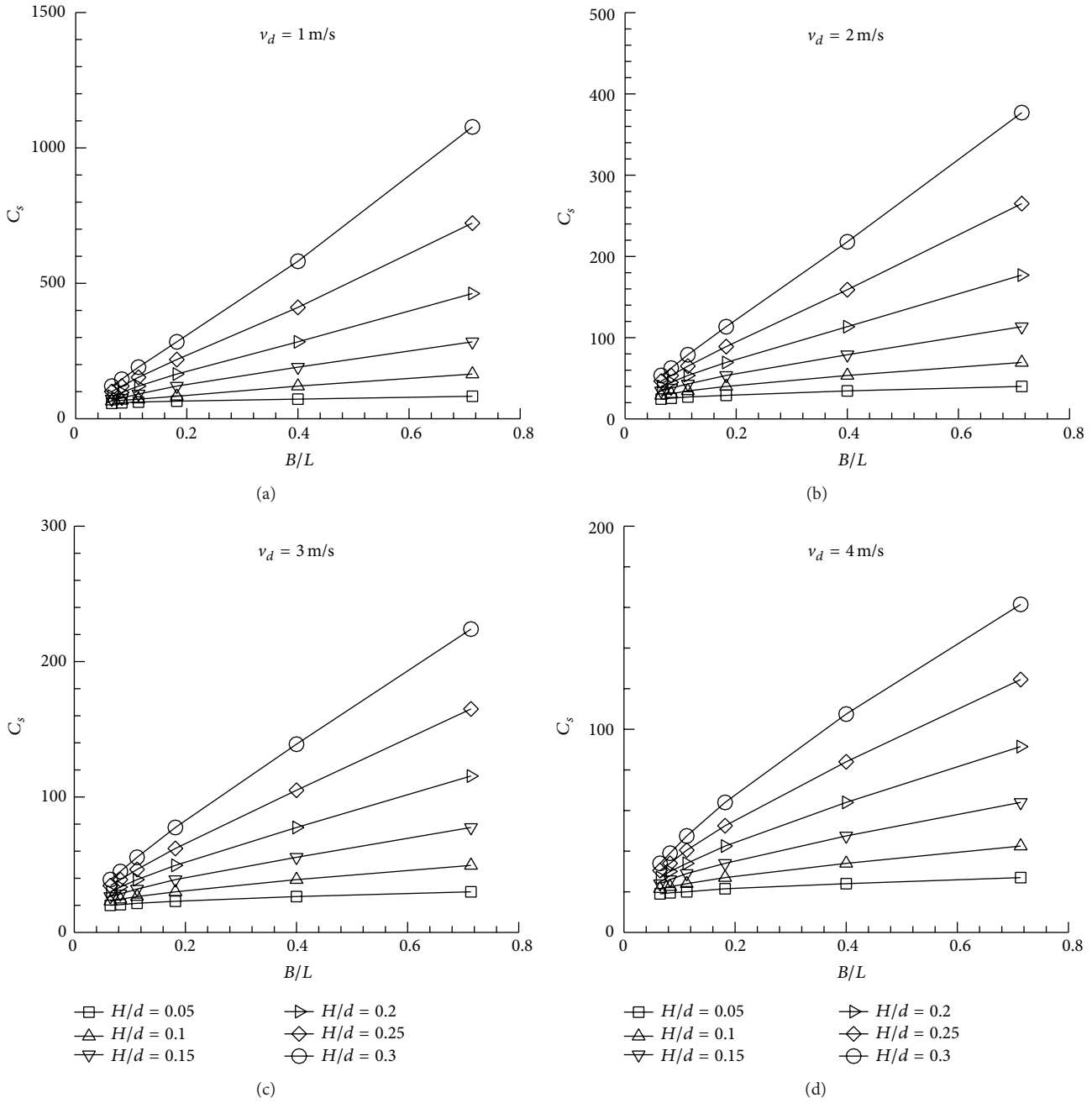

Figure 6: Relationship between slamming coefficient and B/L.

and also provide the foundation for investigating dynamic characteristics of deploying system of ocean structures during deployed body lowering through splash zone.

Conflict of Interests

The authors declare that there is no conflict of interests regarding the publication of this paper.

Acknowledgment

The authors gratefully acknowledge the support of the National Natural Science Foundation of China (no. 51305463).

References

[1] T. Von Karman, "The impact of seaplane floats during landing," TN 321, National Advisory Committee for Aeronautics, 1929.

[2] H. Wanger, "Trans phenomena associated with impacts and sliding on liquid surfaces," *Math Mechanics*, vol. 12, no. 4, pp. 193–215, 1932.

[3] S. L. Chuang, "Experiments on flat-bottom slamming," *Journal of Ship Research*, vol. 10, pp. 10–17, 1966.

[4] R. Zhao and O. Faltinsen, "Water entry of two-dimensional bodies," *Journal of Fluid Mechanics*, vol. 246, pp. 593–612, 1993.

[5] DNV-RP-H103, *Recommended Practice: Modelling and Analysis of Marine Operations*, DET NORSKE VERITAS, Oslo, Norway, 2011.

[6] R. Baarholm and O. M. Faltinsen, "Wave impact underneath horizontal decks," *Journal of Marine Science and Technology*, vol. 9, no. 1, pp. 1–13, 2004.

[7] Z. Chen and X. Xiao, "Simulation analysis on the role of air cushion in the slamming of a flat-bottom structure," *Journal of Shanghai Jiaotong University*, vol. 39, no. 5, pp. 670–673, 2005.

[8] T. Bunnik and B. Buchner, "Numerical prediction of wave loads on subsea structures in the splash zone," in *Proceedings of the 14th International Offshore and Polar Engineering Conference (ISOPE '04)*, pp. 284–290, Toulon, France, May 2004.

[9] T. Bunnik, B. Buchner, and A. Veldman, "The use of a Volume of Fluid (VOF) method coupled to a time domain motion simulation to calculate the motions of a subsea structure lifted through the splash zone," in *Proceedings of the 25th International Conference on Offshore Mechanics and Arctic Engineering (OMAE '06)*, vol. 4, pp. 839–846, Hamburg, Germany, June 2006.

[10] Z. Ding, B. Ren, Y. Wang, and X. Ren, "Experimental study of unidirectional irregular wave slamming on the three-dimensional structure in the splash zone," *Ocean Engineering*, vol. 35, no. 16, pp. 1637–1646, 2008.

[11] A. Sarkar and O. T. Gudmestad, "Splash zone lifting analysis of subsea structures," in *Proceedings of the 29th International Conference on Ocean, Offshore and Arctic Engineering (OMAE '10)*, vol. 1, pp. 303–312, Shanghai, China, June 2010.

[12] J. Y. Zhang, D. J. Li, X. Y. Gao, Q. C. Meng, C. J. Yang, and Y. Chen, "Simulation analysis of deployment and retrieval of junction box used in cabled seafloor observatory," *Ship EngIneering*, vol. 32, no. 6, pp. 53–59, 2010 (Chinese).

[13] H.-C. Chen and K. Yu, "CFD simulations of wave-current-body interactions including greenwater and wet deck slamming," *Computers & Fluids*, vol. 38, no. 5, pp. 970–980, 2009.

[14] W.-H. Wang and Y.-Y. Wang, "Numerical study on cylinder entering water in wave," *Journal of Shanghai Jiaotong University*, vol. 44, no. 10, pp. 1393–1399, 2010 (Chinese).

[15] W.-H. Wang and Y.-Y. Wang, "An essential solution of water entry problems and its engineering applications," *Journal of Marine Science and Application*, vol. 9, no. 3, pp. 268–273, 2010.

[16] X.-Z. Hu, S.-J. Liu, and Y. Li, "2D numerical wave tank simulation for deployment of seafloor mining system," *Journal of Central South University*, vol. 42, no. 2, pp. 246–251, 2011.

[17] X.-Z. Hu and S.-J. Liu, "Numerical simulation of calm water entry of flatted-bottom seafloor mining tool," *Journal of Central South University of Technology*, vol. 18, no. 3, pp. 658–665, 2011.

[18] O. M. Faltinsen, *Sea loads on ships and offshore structure*, Cambridge University Press, 1993.

[19] Z. Chen, X. Xiao, and D.-Y. Wang, "Simulation of flat-bottom structure slamming," *China Ocean Engineering*, vol. 19, no. 3, pp. 385–394, 2005.